

# Improved plasticity of Inconel 718 superalloy fabricated by selective laser melting through a novel heat treatment process

X. Li<sup>a</sup>, J.J. Shi<sup>a</sup>, G.H. Cao<sup>a,\*</sup>, A.M. Russell<sup>b</sup>, Z.J. Zhou<sup>c</sup>, C.P. Li<sup>c</sup>, G.F. Chen<sup>c</sup>

<sup>a</sup> State Key Laboratory of Advanced Special Steel and School of Materials Science and Engineering, Shanghai University, 99 Shangda Road, Shanghai 200444, China

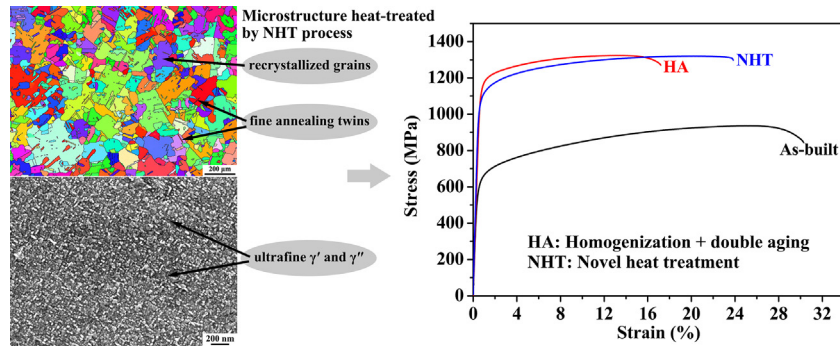
<sup>b</sup> Department of Materials Science and Engineering, Iowa State University and Division of Materials Science and Engineering, Ames Laboratory of the U.S.D.O.E., Ames, IA 50011-2300, USA

<sup>c</sup> Materials & Manufacturing Qualification Group, Corporate Technology, Siemens Ltd., China, Beijing 100102, China

## HIGHLIGHTS

- A novel heat treatment process was proposed for Inconel 718 superalloy.
- The morphology of  $\gamma''$  phase was modified by one-time aging heat treatment.
- The recrystallized grains with annealing twins promoted good plasticity.

## GRAPHICAL ABSTRACT



## ARTICLE INFO

### Article history:

Received 6 May 2019

Received in revised form 31 May 2019

Accepted 3 June 2019

Available online 4 June 2019

### Keywords:

Inconel 718

Selective laser melting

Heat treatment

Plasticity

Annealing twins

## ABSTRACT

When Inconel 718 alloy is fabricated by selective laser melting and treated by traditional homogenization plus double aging heat treatment (HA), its strength improves greatly, but ductility decreases. A novel heat treatment (NHT) including higher temperature homogenization at 1150 °C for 2 h and one-time lower temperature aging treatment at 700 °C for 12 h is developed, which can overcome the strength-plasticity trade-off of Inconel 718 alloy. The results show that recrystallized grains with annealing twins and ultrafine strengthening phases form in the specimen subjected to the NHT. These microstructures differ from those in as-built and conventional heat-treated samples. Especially the morphology of strengthening phase  $\gamma''$ -Ni<sub>3</sub>Nb precipitated in the NHT specimen has changed a lot, it seems to be spherical rather than disc-like shape occurred in the traditional heat-treated samples. Consequently, the NHT process increases plasticity by 41%, while maintaining ultimate strength at the same level achieved by the traditional heat treatment. The enhanced ductility is attributed to the annealing twins and recrystallized grains without local strains, while the strength is provided by the smaller precipitates formed in the NHT one-time aging treatment.

© 2019 The Authors. Published by Elsevier Ltd. This is an open access article under the CC BY-NC-ND license (<http://creativecommons.org/licenses/by-nc-nd/4.0/>).

## 1. Introduction

Inconel 718 (IN718) is a precipitate-strengthened, Ni-Cr-Fe based superalloy, which has been widely used in aerospace components operating at high temperature due to its excellent mechanical properties and

\* Corresponding author.

E-mail address: [ghcao@shu.edu.cn](mailto:ghcao@shu.edu.cn) (G.H. Cao).

good corrosion and oxidation resistance [1,2]. Selective laser melting (SLM) is an additive manufacturing technology developed to fabricate metal parts with complex shape [3]. However, owing to the large thermal gradients and rapid solidification rate during the SLM processing, residual stress and microsegregation could occur, and precipitation of strengthening phases ( $\gamma'$ -Ni<sub>3</sub>(Al,Ti) and  $\gamma''$ -Ni<sub>3</sub>Nb) is suppressed [1,4]. Therefore, post-fabrication heat treatment is critical for SLMed as-built components to mitigate those problems and to obtain sufficient mechanical properties.

The traditional heat treatments include the solution or homogenization plus double aging treatments (SA or HA) commonly used for wrought or cast IN718 samples. Previous investigators have shown improved mechanical performance of SLMed as-built IN718 given such heat treatments [5–7]. The strength increased from these heat treatments is mainly provided by  $\gamma''$  phase of a body centered tetragonal (bct) DO<sub>22</sub> structure, which orientations parallel to [001], [010] and [100] directions. The  $\gamma''$  phases appear disc-shaped in a front view, but they appear acicular in a profile view with length-to-thickness ( $l/t$ ) ratios ranging from ~3 to 13. Although traditional heat treatments can effectively strengthen the materials by introducing nano-scale precipitates, they decrease plasticity. This is often called the strength-plasticity trade-off [8]. Many researchers intend to break through this situation by introducing heterostructures or grain boundary engineering (GBE) method.

It has been noted that twin boundaries can greatly increase mechanical strength, while maintaining good plasticity in aluminium, copper and high-manganese austenitic steels [9–11]. Materials having face centered cubic structure with low stacking-fault energy readily produce annealing twins through thermomechanical treatments [12]. The introduction of annealing twins in materials can be regarded as a kind of GBE technique first proposed by Watanabe [13], which allows one to design the structure and improve properties through modifying the grain boundary character distribution (GBCD). In general, the grain boundaries can be divided into two types: low angle grain boundaries (LAGBs,  $2^\circ \leq \theta < 15^\circ$ ) and high angle grain boundaries (HAGBs,  $\theta > 15^\circ$ ), where  $\theta$  refers to the misorientation angle between adjacent grains. For the HAGBs, the grain boundaries having low coincidence site lattice (CSL) values ( $1 < \Sigma \leq 29$ ) are usually named “special” grain boundaries containing few crystalline defects [14]. Meanwhile, the CSL parameter is widely used to analyze GBCD and identify the twin boundaries. The twinned structure with certain “special” types of boundaries (i.e., coherent CSL  $\Sigma 3$ ) generally alters the energy and mobility of a mobile interface [15], thereby affecting various properties of materials. In addition to the introduction of twin boundaries, some other methods (e.g., controlling the size or morphology of precipitates) have also shown the capability of achieving both high strength and plasticity in materials [16,17].

So far, most researchers have been used to choose the traditional heat treatment methods for SLMed IN718 alloy, indicating that the current heat treatment approaches are limited. In an attempt to achieve both high strength and high ductility in SLMed IN718 alloy, a novel heat treatment (NHT) scheme different from traditional methods was applied to SLMed IN718 samples. The microstructure and mechanical properties of the as-built, HA and NHT samples were studied and compared. Such a study is expected to explore a more effective heat treatment schedule for SLMed IN718 productions.

## 2. Experimental procedure

The IN718 samples were fabricated using an EOSINT-M280 SLM machine consisting of a YLR-400 fiber laser with a maximum output energy of ~400 W. The chemical composition (wt%) of IN718 alloy analyzed by inductively coupled plasma atomic emission spectrometry is 51.9Ni-18.8Cr-5.5Nb-3.9Mo-1.1Ti-0.6Al-Fe (balance). Argon is used as protective gas during the whole process and detailed forming parameters were described in our previous paper [18]. Two kinds of heat treatment

routes shown in Fig. 1a were employed for comparison to the SLMed as-built sample. One is homogenization plus double aging treatment (HA), which is the normal regime widely used for wrought or cast IN718 alloy: 1065 °C × 1.5 h/air cooling (AC) + 760 °C × 10 h/furnace cooling (FC) to 650 °C at the rate of 55 °C/h, and then holding for 8 h/AC to room temperature. The other is the novel heat treatment (NHT) scheme developed in this study (homogenization plus one-time aging approach): homogenizing at 1150 °C for 2 h, followed by AC, then aging at 700 °C for 12 h, and finally water cooling. The homogenization under higher temperature in NHT process is to allow the sample to occur complete recrystallization and produce annealing twins, which could modify the grain boundary character distribution. Based on the Time-Temperature-Transformation (TTT) curve made by Brooks and Bridges [19], as shown in Fig. 1b, the  $\gamma''$  phase precipitating before  $\gamma'$  phase has a large precipitation range from 600 to 900 °C. The temperature and exposed time of the one-time aging treatment (700 °C/12 h) applied in the NHT method are lower and shorter than those used in the double aging treatments, respectively, which is expected to precipitate the  $\gamma''$  phase with smaller size in the NHT sample.

Specimens cut by electro-discharge machining (EDM) were ground successively from 400 grit to 2500 grit, and then mechanically polished by using diamond suspension of 2  $\mu$ m to 0.5  $\mu$ m and colloidal silica suspension of 0.05  $\mu$ m. After polishing, the samples were subjected to electrolytic corrosion (etched in a solution of 70 vol% phosphoric acid and 30 vol% H<sub>2</sub>O at 5 V for 10–20 s). The microstructural characterization was completed by a JSM-7001F scanning electron microscopy (SEM) and a JEM 2100F transmission electron microscopy (TEM). The crystallographic information of grains was examined by an electron backscatter diffraction (EBSD) system with step size of 2.5  $\mu$ m and the EBSD data were analyzed using Oxford HKL Channel 5 software. Tensile specimens having gauge dimensions of 4 × 1 × 14 mm were cut by EDM and stretched on a MTS C40 electronic universal testing machine equipped with an Epsilon 3442 electronic extensometer at room temperature. Each series of the as-built, HA and NHT specimens was conducted three times for tensile testing and the average values were obtained. All the characterized surfaces of specimens were the horizontal section (XY plane) perpendicular to the building direction during the SLM process.

## 3. Results

An EBSD map showing grain morphology and orientation in an as-built SLMed IN718 sample is shown in Fig. 2a. Owing to its layer-by-layer fabrication strategy, SLM processing is similar to directional solidification, resulting in equiaxed grains with {001} texture in the XY plane. The average grain size of the as-built sample was measured to be about 20  $\mu$ m based on the EBSD data. There are also many fine cellular substructures (shown in Fig. 2b) present in the individual grains with nearly the same crystallographic orientation. Their presence is ascribed to the rapid solidification rate of 10<sup>5</sup>–10<sup>7</sup> K/s during the forming process [20]. A high magnification TEM bright field image (Fig. 2c) displays a high dislocation density caused by residual stress in the as-built sample. Aside from some irregular block-shaped Laves phases pinned at the substructure's boundaries, no other precipitates such as  $\gamma'$  and  $\gamma''$  phases can be observed, the rapid solidification rate may inhibit their precipitation. It can be seen from Fig. 2d that the grain size, the morphology and orientation of the HA specimen differ little from those in the as-built sample. However, the nano-scale  $\gamma'$  and  $\gamma''$  precipitates are exhibited in the  $\gamma$  austenite, and the coarser Laves phases still lie on the grain boundaries, as shown in Fig. 2e. Close observation (Fig. 2f) of the region in Fig. 2e (marked with a dashed yellow square) shows uniformly distributed spherical  $\gamma'$  particles of ~50 nm in diameter and disc-like  $\gamma''$  phases (appearing like a strip from the side view) with length range from 100 to 400 nm and their thickness is about 30 nm, and the  $l/t$  ratio of the  $\gamma''$  phases is 3–13.

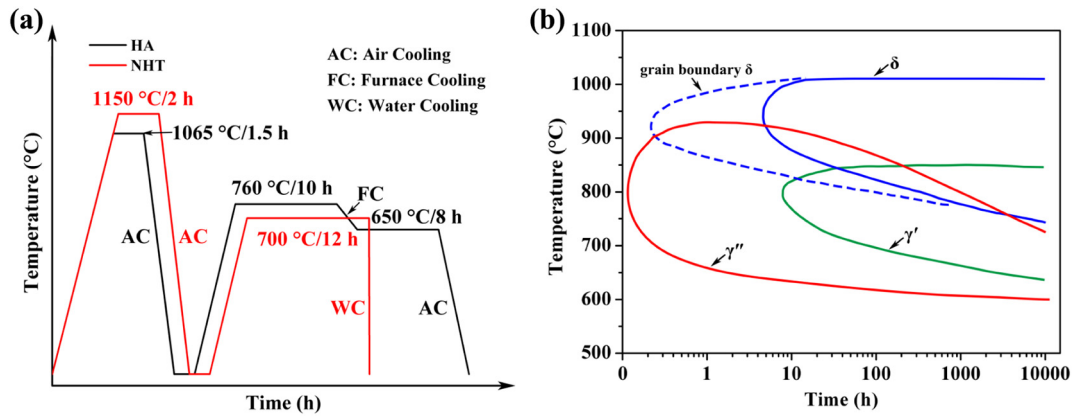


Fig. 1. (a) Schematic illustrations of heat treatment routes: homogenization plus double aging (HA), novel heat treatment (NHT), and (b) TTT diagram of different phases in Inconel 718 alloy [19].

Fig. 3a represents the orientation image EBSD map of the NHT specimen. It can be observed that the initial equiaxed microstructures of the as-built specimen are replaced by uniform recrystallized grains with random crystallographic orientations. Some of the recrystallized grains are relatively coarse, and the average grain size is measured to be about 65 μm, which is larger than those of the as-built and HA specimens. In addition, a great deal of fine annealing twins indicated by arrows are also observed in the NHT specimen. Fig. 3b is a SEM image showing that few Laves phases are present at the grain boundaries. In order to identify the ultrafine precipitates in the matrix, the highly magnified Fig. 3c enlarges the region marked by the yellow rectangle in Fig. 3b, illustrating the morphologies and distributions of the γ' and γ'' phases. It is noteworthy that the γ' and γ'' precipitates with size of 10–35 nm are both much smaller than those in the HA specimen. Especially, the γ'' phases are observed to be circular rather than the previously seen disc-like shape, and the *l/t* ratio falls to 1–3. It is difficult to distinguish the γ' and γ'' phases through SEM owing to their similar sizes and shapes. Therefore, TEM is required for better and deeper understanding. Fig. 4a is the selected area electron diffraction (SAED)

patterns from the γ matrix and ultrafine precipitates. According to the SAED, those circular precipitates were identified as γ'' phases with a bct DO<sub>22</sub> crystal structure. Fig. 4b is a dark field image from the diffraction (110) spot of γ'', which is marked by yellow circle in the Fig. 4a, confirming the presence of γ'' phases in the matrix of NHT specimen. The crystallographic orientation relationship of γ'' with γ obeys (100)[001]γ''//((100)[001]γ).

Fig. 5a–c displays the local misorientation (LM) maps of the as-built, HA and NHT specimens, respectively. The LM is a parameter calculated from the EBSD data to assess strain distribution as well as dislocation density [21]. In the LM map, the blue and red represent the lowest and highest dislocation density, respectively. Heterogeneous LM distributions are presented in the as-built and HA specimens, and higher strain or dislocation density concentrate near the grain boundaries where the Laves phases lie. However, the NHT sample with recrystallized grains has lower dislocation density. The LM values vs. relative frequency are shown in Fig. 5d. It can be observed that the values of the as-built and HA specimens are almost equal, while the NHT specimen possesses a much lower value (close to 0.2).

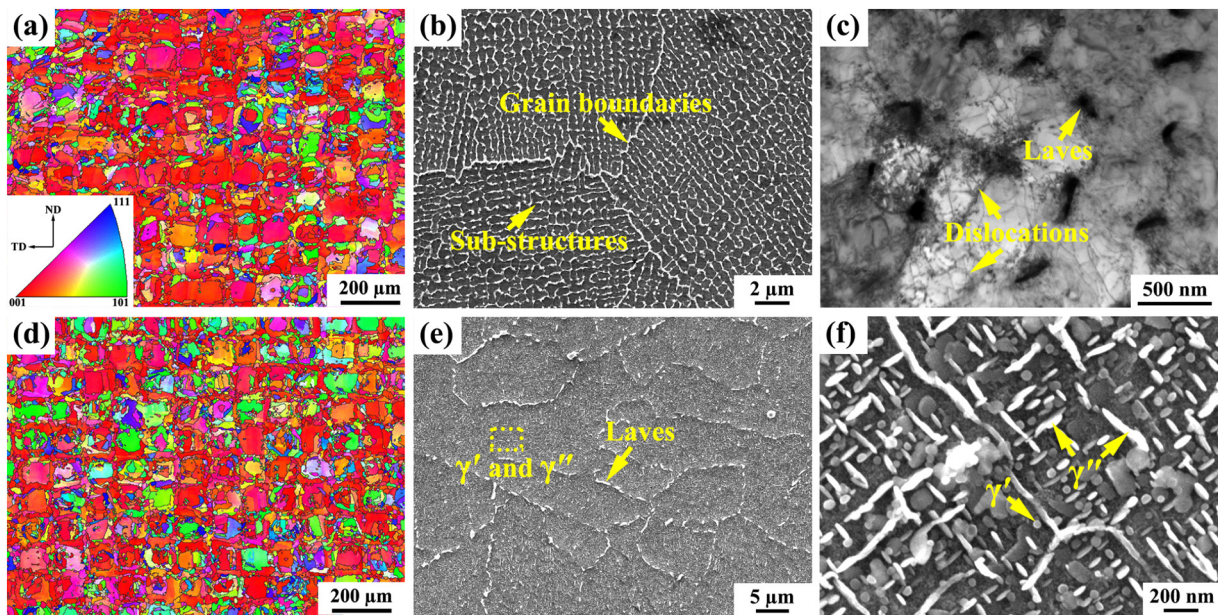
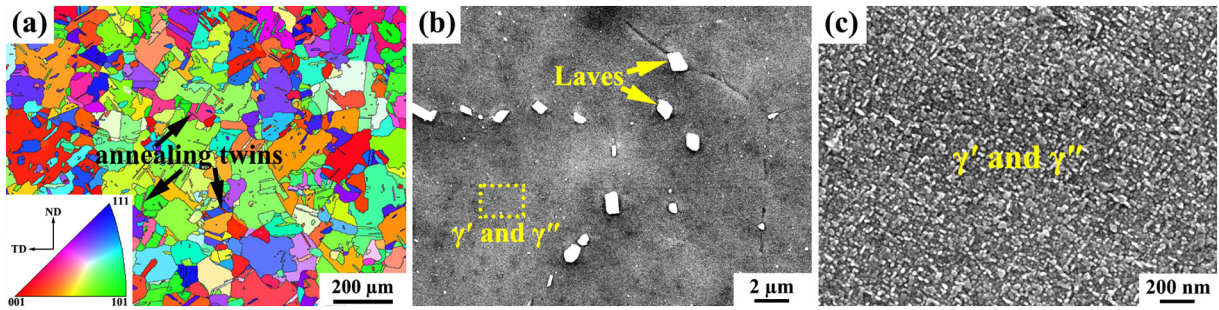


Fig. 2. (a) EBSD orientation image map indicating the grains morphology and texture, the inset is the inverse pole figure, (b) SEM image showing the sub-structures and (c) TEM bright field image displaying the Laves phases and dislocations of the as-built sample; (d) EBSD orientation image map, (e) SEM image showing the precipitates at the grain boundaries or within the γ austenite of the HA specimen, and (f) the corresponding high magnification of the dashed-line yellow rectangle region marked in (e).



**Fig. 3.** (a) EBSD orientation image map of the NHT specimen, the inset is the inverse pole figure, (b) SEM micrograph showing the Laves phase at the grain boundaries, and (c) the corresponding high magnification of yellow rectangle region in (b).

With the exception of LM values, the CSL values of three specimens are also different. Fig. 6a–c shows CSL grain boundaries distribution maps of the as-built, HA and NHT specimens, respectively. It should be noted that the black lines represent the general grain boundaries and the red lines correspond to the CSL  $\Sigma 3$  grain boundaries. It is observed that the general grain boundaries dominate in the as-built and HA specimens, while the special grain boundaries (especially the  $\Sigma 3$  twin boundaries) prevail after the NHT process, occupying a very large proportion. Fig. 6d shows the relative number fractions of different CSL grain boundaries in the three kinds of specimens. A high fraction of CSL  $\Sigma 3$  (up to 65%) is present in the NHT specimen, which resulted from the annealing twins suggesting GBCD optimization. As for the as-built and HA specimens, their relative frequencies of CSL grain boundaries are nearly identical and quite low. The results strongly imply that as long as the samples follow suitable thermal activation (i.e. NHT), the grain boundaries network of SLMed IN718 alloy could be engineered via introducing annealing twins during the recrystallization process. Holland et al. [22] also found this similar phenomenon, the grain boundary character distribution and connectivity of grain boundary network in the heat-treated samples with annealing twins are quite different from those in the as-built sample.

Fig. 7 shows the room temperature tensile stress-strain curves of three specimens. The colored scattered points representing the ultimate strengths and elongations from the references are also given for comparison [6,7,23–27]. The detailed mechanical properties values are listed in the Table 1. The as-built sample exhibits the lowest tensile strength (935 MPa) and the largest plasticity strain (30%) among of investigated specimens. Increased ultimate strength (1325 MPa) and decreased elongation to fracture (17%) were induced by HA treatment. When heat-treated with NHT, the yield strength was a little lower than that of HA specimen, the ultimate strength was similar (1320 MPa), and the plasticity (24%) improved substantially, which is

also much higher than the plasticity reported by other researchers using SLM processing [6,7,23–27].

#### 4. Discussion

Fine grains and few Laves phases dominate in the as-built sample. Their dislocations are thought to glide and multiply freely during deformation, contributing to high ductility but inferior strength owing to the absence of strengthening phases. For the HA specimen, the homogenization at 1065 °C hardly affects the grain size, morphology, dislocation density and GBCD; it merely eliminates the microsegregation induced by SLM fabrication. The subsequent double aging treatments (first stage at 760 °C/10 h and second stage at 650 °C/8 h) are able to precipitate uniform  $\gamma'$  and  $\gamma''$  phases, which would be expected to interact strongly with dislocations. And the  $\gamma''$  phase plays a more significant strengthening role due to its larger misfit with  $\gamma$ . It was reported that the misfits of coherent  $\gamma'$  and  $\gamma''$  phases with  $\gamma$  matrix are 0.4% and 2–3% [28], respectively, the yield and ultimate strengths increase greatly, but plasticity decreases at the same time in the HA specimen.

The NHT specimen shows a different grain morphology (Fig. 3a) in comparison with the as-built and HA specimens. Homogenization at 1150 °C for 2 h provides more activation energy for grain boundary migration. In addition, with the residual stress caused by SLM processing as a driving force, recrystallization occurs more easily in the NHT specimen. Meanwhile, a high volume fraction of annealing twins (Fig. 3a) is formed within the recrystallized grains due to the migration of HAGBs, whose nucleation is attributed to the packets of overlapping stacking faults or growth accidents [29,30]. A large number of CSL  $\Sigma 3$  with HAGBs shown in Fig. 6d is also an indication of the annealing twins in the NHT specimen. It is worthy to mention that the formation of the annealing twins in materials with low stacking fault energy is

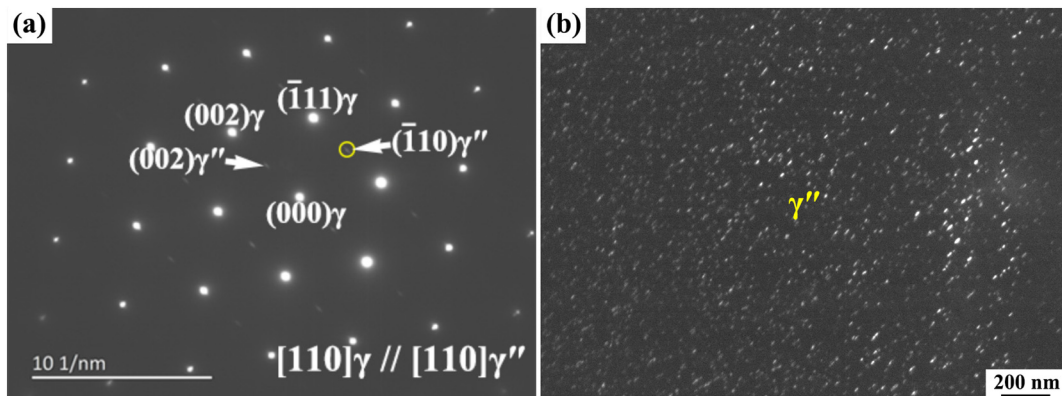


**Fig. 4.** (a) The SAED patterns of the  $\gamma$  and  $\gamma''$  phases along  $[110]$  zone axes and (b) the TEM dark field image from the marked diffraction  $(\bar{1}10)$  spot of  $\gamma''$  phase.

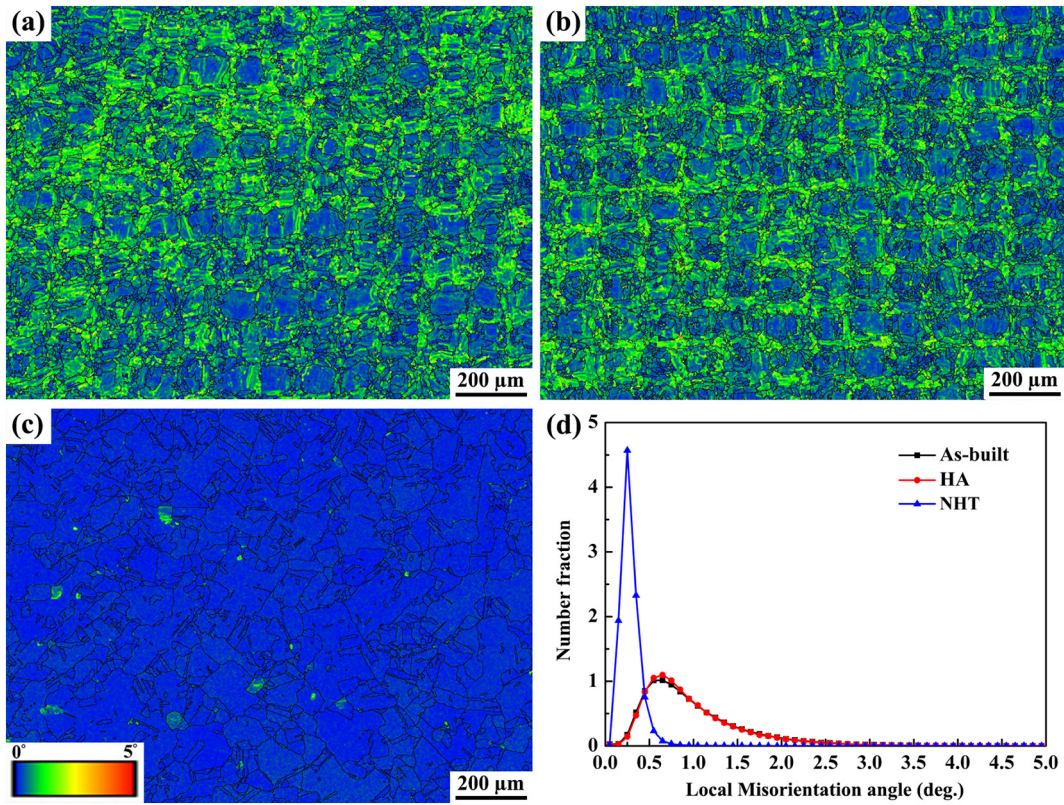


Fig. 5. Local misorientation (LM) maps of the analyzed areas in the (a) as-built, (b) HA, and (c) NHT specimens, respectively, and (d) LM vs. number fraction of the different specimens.

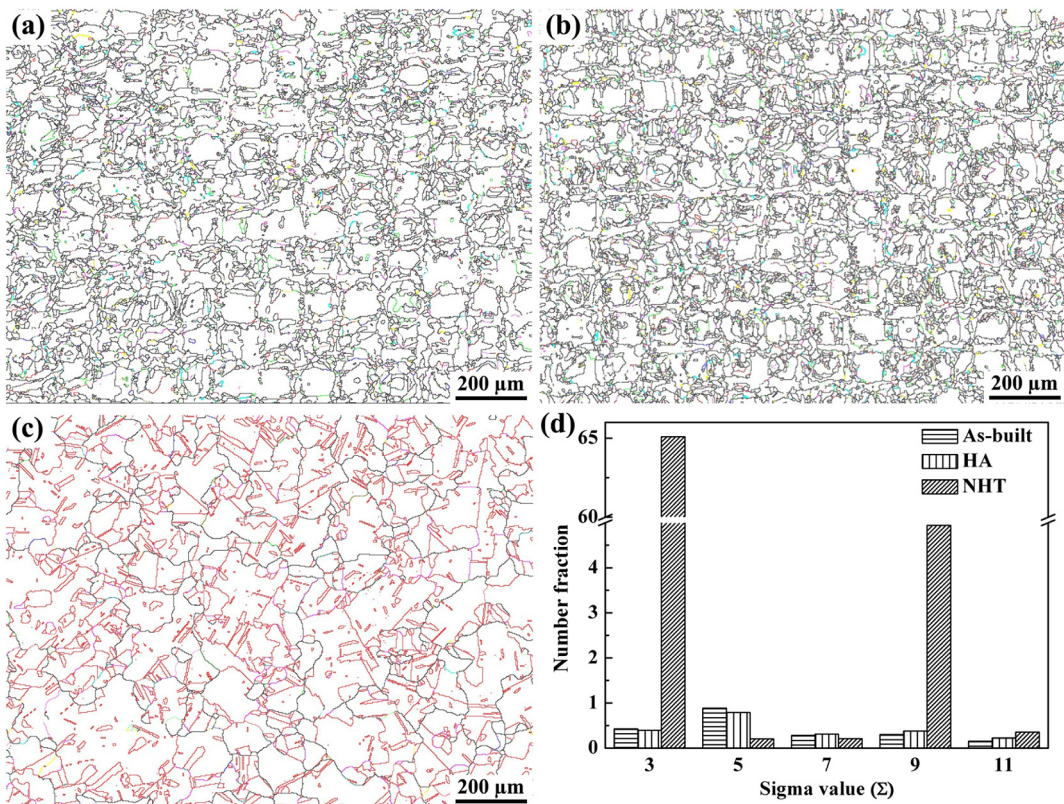


Fig. 6. Coincidence site lattice (CSL) grain boundaries distribution maps of the analyzed areas in the (a) as-built, (b) HA, and (c) NHT specimens, respectively, and (d) CSL value vs. number fraction of the different specimens.

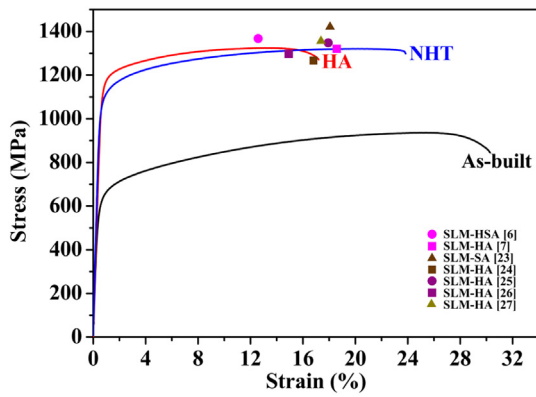


Fig. 7. Stress-strain curves of the as-built, HA and NHT specimens at room temperature.

not only a product of the recrystallized grains, but also promotes the recrystallization process in turn [15]. Xue et al. [31] found that HAGBs are able to hinder and block the dislocations effectively, which contribute to enhance the strain-hardening capacity and improve the ductility of materials. Some other researchers have also revealed that the reasonable plasticity can be obtained by the sliding of the HAGBs [32,33]. Therefore, it is easy to understand that the plasticity of the NHT specimen is increased by annealing twin boundaries with CSL  $\Sigma 3^n$ . On the other hand, the NHT specimen has a relatively low dislocation density shown in the Fig. 5c and d, which is caused by the recrystallization process, providing more free room for further dislocation storage. Thus, the NHT specimen has a higher elongation to fracture (24%) than that of the HA specimen (17%).

Though the plasticity of the NHT specimen can be enhanced by the annealing twins and recrystallized structures, its strength might be decreased by the relatively coarser recrystallized grains ( $\sim 65 \mu\text{m}$ ) compared with equiaxed finer grains ( $\sim 20 \mu\text{m}$ ) in the as-built and HA specimens. In order to solve this problem, ultrafine strengthening precipitates are introduced via the subsequent aging treatment. Unlike the double aging treatments used in the HA specimen, here it is only subjected to one-time aging treatment at a temperature of  $700^\circ\text{C}$  for 12 h in the NHT specimen. This temperature is lower than the  $760^\circ\text{C}$  used for the first aging stage during the double aging treatments (20 h in total) of the HA specimen. Actually, in accordance with the TTT curve made by Brooks and Bridges [19], it is able to precipitate  $\gamma'$  and  $\gamma''$  phases when aging at a temperature of  $700^\circ\text{C}$ . Han et al. indicated that the growth of a precipitate is controlled by diffusion and activation energy, which is named Lifshitz-Wagner theory [28]. Owing to the relatively lower aging temperature ( $700^\circ\text{C}$ ) and shorter exposed time (12 h), the  $\gamma''$  phases in the NHT specimen have a lower growth rate, resulting in smaller size (10–35 nm) than the  $\gamma''$  phases of 100–400 nm in the HA specimen. And the water cooling that follows helps to preserve the metastable  $\gamma''$  phase. Such a phenomenon was also observed by Han et al. [28] and Slama et al. [34]. The ultrafine  $\gamma''$

Table 1

Yield strength (YS), tensile strength (UTS) and elongation to failure ( $\epsilon_f$ ) values of the as-built and heat-treated specimens.

Material conditions	YS (MPa)	UTS (MPa)	$\epsilon_f$ (%)
As-built	590 $\pm$ 5	935 $\pm$ 16	30 $\pm$ 3
HA	1100 $\pm$ 15	1325 $\pm$ 19	17 $\pm$ 2
NHT	1070 $\pm$ 12	1320 $\pm$ 14	24 $\pm$ 1
HSA <sup>a</sup> by ref. [6]	1046	1371	12.3
HA by ref. [7]	1074	1320	19.0
SA by ref. [23]	1185	1430	18.6
HA by ref. [24]	1065	1272	16.5
HA by ref. [25]	1110	1335	18.0
HA by ref. [26]	1100	1315	15.0
HA by ref. [27]	1160	1350	17.6

<sup>a</sup> HSA: Homogenization + Solution + Double aging treatments.

phases have strong interactions with dislocations during the tensile deformation and provide coherent lattice distortions, making up for the loss of strength caused by coarser recrystallized grains in the NHT specimen. Therefore, the ultimate strength is nearly equal to that of the HA specimen (1325 MPa).

## 5. Conclusions

A novel heat treatment (NHT) scheme was proposed for SLMed Inconel 718 superalloy. The microstructure and mechanical properties of the as-built, HA and NHT samples have been studied. The specimen treated by NHT in this research achieved an enhanced strength-ductility synergy, which can't be obtained via the traditional HA treatment. The elongation to fracture is improved greatly from 17% to 24% with little loss of ultimate strength (1325 MPa vs. 1320 MPa). The recrystallized grains with annealing twins promote good plasticity, while the finer  $\gamma'$  and  $\gamma''$  precipitates maintain a high level of strength.

## Data availability

The data that support the findings of this study are available from the corresponding author upon reasonable request.

## CRedit authorship contribution statement

**X. Li:** Methodology, Investigation, Writing - original draft. **J.J. Shi:** Writing - review & editing. **G.H. Cao:** Project administration, Resources, Supervision, Writing - review & editing. **A.M. Russell:** Writing - review & editing. **Z.J. Zhou:** Writing - review & editing. **C.P. Li:** Writing - review & editing. **G.F. Chen:** Writing - review & editing.

## CRedit authorship contribution statement

**X. Li:** Methodology, Investigation, Writing - original draft. **J.J. Shi:** Writing - review & editing. **G.H. Cao:** Project administration, Resources, Supervision, Writing - review & editing. **A.M. Russell:** Writing - review & editing. **Z.J. Zhou:** Writing - review & editing. **C.P. Li:** Writing - review & editing. **G.F. Chen:** Writing - review & editing.

## Acknowledgment

This work was financially supported by Siemens Ltd., China, the Shanghai Committee of Science and Technology, China, under Grant no. 11520701200, and the National Natural Science Foundation of China (NSFC) under Grant no. 51271107.

## References

- [1] K.N. Amato, S.M. Gaytan, L.E. Murr, E. Martinez, P.W. Shindo, J. Hernandez, S. Collins, F. Medina, Microstructures and mechanical behavior of Inconel 718 fabricated by selective laser melting, *Acta Mater.* 60 (2012) 2229–2239.
- [2] D.C. Lv, D. Mcallister, M.J. Mills, Y. Wang, Deformation mechanisms of DO<sub>22</sub> ordered intermetallic phase in superalloys, *Acta Mater.* 118 (2016) 350–361.
- [3] T. DebRoy, H.L. Wei, J.S. Zuback, T. Mukherjee, J.W. Elmer, J.O. Milewski, A.M. Beese, A. Wilson-Heid, A. De, W. Zhang, Additive manufacturing of metallic components—process, structure and properties, *Prog. Mater. Sci.* 92 (2018) 112–224.
- [4] B. Vrancken, V. Cain, R. Knutsen, J.V. Humbeeck, Residual stress via the contour method in compact tension specimens produced via selective laser melting, *Scr. Mater.* 87 (2014) 29–32.
- [5] Y.L. Kuo, S. Horikawa, K. Takehi, Effects of build direction and heat treatment on creep properties of Ni-base superalloy built up by additive manufacturing, *Scr. Mater.* 129 (2017) 74–78.
- [6] D.Y. Zhang, W. Niu, X.Y. Cao, Z. Liu, Effect of standard heat treatment on the microstructure and mechanical properties of selective laser melting manufactured Inconel 718 superalloy, *Mater. Sci. Eng. A* 644 (2015) 32–40.
- [7] E. Chlebus, K. Gruber, B. Kuźnicka, J. Kurzac, T. Kurzynowski, Effect of heat treatment on the microstructure and mechanical properties of Inconel 718 processed by selective laser melting, *Mater. Sci. Eng. A* 639 (2015) 647–655.
- [8] B. Berman, 3-D printing: the new industrial revolution, *Bus. Horiz.* 55 (2012) 155–162.

- [9] D. Bufford, Y. Liu, J. Wang, H. Wang, X. Zhang, In situ nanoindentation study on plasticity and work hardening in aluminium with incoherent twin boundaries, *Nat. Commun.* 5 (2014) 4864.
- [10] L. Lu, Y.F. Shen, X.H. Chen, L.H. Qian, K. Lu, Ultrahigh strength and high electrical conductivity in copper, *Science* (304) (2004) 422–426.
- [11] O. Bouaziz, S. Allain, C.P. Scott, P. Cugy, D. Barbier, High manganese austenitic twinning induced plasticity steels: a review of the microstructure properties relationships, *Curr. Opin. Solid State Mater. Sci.* 15 (2011) 141–168.
- [12] T.S. Prithiv, P. Bhuyan, S.K. Pradhan, V.S. Sarma, S. Mandal, A critical evaluation on efficacy of recrystallization vs. strain induced boundary migration in achieving grain boundary engineered microstructure in a Ni-base superalloy, *Acta Mater.* 146 (2018) 187–201.
- [13] T. Watanabe, An approach to grain-boundary design for strong and ductile polycrystals, *Res. Mech.* 11 (1984) 47–84.
- [14] G. Palumbo, K.T. Aust, E.M. Lehochey, U. Erb, P. Lin, On a more restrictive geometric criterion for special CSL grain boundaries-atomic level structure and properties, *Scr. Mater.* 38 (1998) 1685–1690.
- [15] D.P. Field, L.T. Bradford, M.M. Nowell, T.M. Lillo, The role of annealing twins during recrystallization of Cu, *Acta Mater.* 55 (2007) 4233–4241.
- [16] S.H. Kim, H. Kim, N.J. Kim, Brittle intermetallic compound makes ultrastrong low-density steel with large ductility, *Nature* 518 (2015) 77–79.
- [17] S. Cheng, Y.H. Zhao, Y.T. Zhu, E. Ma, Optimizing the strength and ductility of fine structured 2024 Al alloy by nano-precipitation, *Acta Mater.* 55 (2007) 5822–5832.
- [18] X. Li, J.J. Shi, C.H. Wang, G.H. Cao, A.M. Russell, Z.J. Zhou, C.P. Li, G.F. Chen, Effect of heat treatment on microstructure evolution of Inconel 718 alloy fabricated by selective laser melting, *J. Alloys Compd.* 764 (2018) 639–649.
- [19] J.W. Brooks, P.J. Bridges, Metallurgical stability of Inconel alloy 718, *Superalloys 88* (1988) 33–42.
- [20] J.P. Choi, G.H. Shin, S.S. Yang, D.Y. Yang, J.S. Lee, M. Brochu, J.H. Yu, Densification and microstructural investigation of Inconel 718 parts fabricated by selective laser melting, *Powder Technol.* 310 (2017) 60–66.
- [21] M. Kamaya, Measurement of local plastic strain distribution of stainless steel by electron backscatter diffraction, *Mater. Charact.* 60 (2009) 125–132.
- [22] S. Holland, X. Wang, X.Y. Fang, Y.B. Guo, F. Yan, L. Li, Grain boundary network evolution in Inconel 718 from selective laser melting to heat treatment, *Mater. Sci. Eng. A* 725 (2018) 406–418.
- [23] T. Trosch, J. Strößner, R. Völkl, U. Glatzel, Microstructure and mechanical properties of selective laser melted Inconel 718 compared to forging and casting, *Mater. Lett.* 164 (2016) 428–431.
- [24] V.A. Popovich, E.V. Borisov, A.A. Popovich, V.S. Sufiarov, D.V. Masaylo, L. Alzina, Impact of heat treatment on mechanical behaviour of Inconel 718 processed with tailored microstructure by selective laser melting, *Mater. Des.* 131 (2017) 12–22.
- [25] S. Raghavan, B.C. Zhang, P. Wang, C.N. Sun, M.L. Nai, T. Li, J. Wei, Effect of different heat treatments on the microstructure and mechanical properties in selective laser melted Inconel 718 alloy, *Mater. Manuf. Process.* 32 (2017) 1588–1595.
- [26] M.E. Aydinöz, F. Brenne, M. Schaper, C. Schaak, W. Tillmann, J. Nellesen, T. Niendorf, On the microstructural and mechanical properties of post-treated additively manufactured Inconel 718 superalloy under quasi-static and cyclic loading, *Mater. Sci. Eng. A* 669 (2016) 246–258.
- [27] A.A. Popovich, V.S. Sufiarov, I.A. Polozov, E.V. Borisov, Microstructure and mechanical properties of Inconel 718 produced by SLM and subsequent heat treatment, *Key Eng. Mater.* 653 (2015) 665–670.
- [28] Y.F. Han, P. Deb, M.C. Chaturvedi, Coarsening behaviour of  $\gamma''$  and  $\gamma'$  particles in Inconel alloy 718, *Met. Sci.* 16 (1982) 555–562.
- [29] S. Mahajan, Critique of mechanisms of formation of deformation, annealing and growth twins: face-centered cubic metals and alloys, *Scr. Mater.* 68 (2013) 95–99.
- [30] S. Mahajan, C.S. Pande, M.A. Imam, B.B. Rath, Formation of annealing twins in fcc crystals, *Acta Mater.* 45 (1997) 2633–2638.
- [31] P. Xue, B.L. Xiao, Z.Y. Ma, Enhanced strength and ductility of friction stir processed Cu–Al alloys with abundant twin boundaries, *Scr. Mater.* 68 (2013) 751–754.
- [32] Y.H. Zhao, Y.T. Zhu, E.J. Lavernia, Strategies for improving tensile ductility of bulk nanostructured materials, *Adv. Eng. Mater.* 12 (2010) 769–778.
- [33] N.Q. Chinh, P. Szommer, Z. Horita, T.G. Langdon, Experimental evidence for grain-boundary sliding in ultrafine-grained aluminum processed by severe plastic deformation, *Adv. Mater.* 18 (2006) 34–39.
- [34] C. Slama, M. Abdellaoui, Structural characterization of the aged Inconel 718, *J. Alloys Compd.* 306 (2000) 277–284.